

Quantum mechanical heat transport in disordered harmonic chains

Christopher Gaul* and Helmut Büttner

Physikalisches Institut, Universität Bayreuth, D-95440 Bayreuth, Germany

We investigate the mechanism of heat conduction in ordered and disordered harmonic onedimensional chains within the quantum mechanical Langevin method. In the case of the disordered chains we find indications for normal heat conduction which means that there is a finite temperature gradient but we cannot clearly decide whether the heat resistance increases linearly with the chain length. Furthermore we observe characteristic quantum mechanical features like Bose–Einstein statistics of the occupation numbers of the normal modes, freezing of the heat conductivity and the influence of the entanglement within the chain on the current. For the ordered chain we recover some classical results like a vanishing temperature gradient and a heat flux independent of the length of the chain.

PACS numbers: 44.10.+i, 05.10.Gg, 05.60.Gg

I. INTRODUCTION

Fourier’s law of heat conduction states that the heat flux j_Q through a medium is proportional to the temperature gradient: $j_Q = -\kappa \nabla T$. This implies for the stationary, one dimensional case, where the heat flux is homogeneous, that the temperature gradient must be constant, as well, at least if the thermal conductivity κ is not temperature dependent. However it is highly non-trivial to deduce Fourier’s law from either classical or quantum mechanical statistical physics.

In 1955 Fermi, Pasta and Ulam [1] performed the first numerical calculations on the dynamics of harmonic chains, the simplest imaginable model for lattice vibrations in insulators. They found that harmonic chains do not find their way to equilibrium because the normal modes are decoupled in harmonic systems. In one dimensional ordered chains the heat flux is independent of the length of the chain and the temperature gradient vanishes. In disordered chains the conductivity is reduced due to the Anderson localization of most of the normal modes. Although there is a finite temperature gradient, the overall resistance does not increase linearly with the chain length, but is proportional to the square root of the length [2]. That means that the specific conductivity still diverges with length. Non-integrability is necessary for the observation of equilibration of energy and diffusive heat conduction as described by Fourier’s law. The problem of heat conductivity in all kinds of model systems has been an active field of research for decades [3, 4, 5]. Still there exists no model Hamiltonian system for which Fourier’s law has been proven rigorously.

The one dimensional case is easiest to handle and can be partly justified as a model of the homogeneous three dimensional case. However heat diffusion perpendicular to the direction of the heat flux is neglected. This can be compensated with self-consistent heat baths, which add noise and damping with zero average energy flux to every

site of the chain. Bonetto, Lebowitz and Lukkarinen find normal heat conductivity in such a model [6].

The other side of the problem is the quantum mechanical description of temperature and heat which include thermal fluctuations and dissipation. To achieve this we follow the ansatz by Ullersma [7, 8] and extend the considered system by introducing a heat bath consisting of many environment degrees of freedom. This degrees of freedom will be traced out and a Langevin equation is obtained. The energy transfer from the system into the bath degrees of freedom appears as a damping term. Reversely the initial conditions of the bath degrees of freedom appear as a noise term.

The aim of this work is to use the quantum mechanical Langevin ansatz for heat conduction in a chain. For technical reasons we restrict ourselves to one dimensional harmonic systems without self-consistent heat baths in the ordered as well as in the disordered case. Recently Dhar and Roy [9] have followed the same ansatz in a slightly different form. They apply their method to the self-consistent heat bath model [6].

Alternative systems for the investigation of quantum mechanical heat conduction are systems of coupled spins [10, 11]. The main difference compared to harmonic oscillators is the finite dimensional Hilbert space with e. g. only two energy levels per site for spin- $\frac{1}{2}$. Depending on the types of coupling and of the choice of parameters normal heat conduction is found or not.

II. MODELS FOR HEAT CONDUCTION

A. Disordered harmonic chain coupled to two heat baths

We consider a chain consisting of l harmonic oscillators. X_j and P_j denote the coordinate and the momentum of the j -th oscillator. The oscillators have common mass M but each oscillator has its own onsite frequency ω_j . Nearest neighbors X_j and X_{j+1} are coupled via the

*Electronic address: christopher.gaul@uni-bayreuth.de

coupling constant f_j .

$$H_{\text{ch}} = \sum_{j=1}^l \left(\frac{P_j^2}{2M} + \frac{1}{2} M \omega_j^2 X_j^2 \right) + \sum_{j=1}^{l-1} \frac{f_j}{2} (X_j - X_{j+1})^2 \quad (1)$$

There are two heat baths denoted by a and b which are coupled to the first and to the last oscillator via coupling constants c_i .

$$H_a = \sum_{i=1}^N \left[\frac{p_{ai}^2}{2m_i} + \frac{1}{2} m_i \omega_i^2 \left(x_{ai} - \frac{c_i}{m_i \omega_i^2} X_1 \right)^2 \right] \quad (2)$$

$$H_b = \sum_{i=1}^N \left[\frac{p_{bi}^2}{2m_i} + \frac{1}{2} m_i \omega_i^2 \left(x_{bi} - \frac{c_i}{m_i \omega_i^2} X_l \right)^2 \right] \quad (3)$$

The Hamiltonian of the complete system is then

$$H = H_{\text{ch}} + H_a + H_b. \quad (4)$$

Initially the bath degrees of freedom are independently occupied according to the bath temperatures T_a and T_b . The normal coordinates of the isolated chain are occupied according to the temperature T_{ch} . Then the couplings c_i are switched on at time $t = 0$.

1. The equations of motion

Regarding $X_1(t)$ and $X_l(t)$ as known inhomogeneities, the equations of motion for the bath degrees of freedom are solved and substituted into the equations of motion for the chain. One gets the quantum mechanical Langevin equations [17]

$$\begin{aligned} \ddot{X}_j(t) = & -C_{jk} X_k(t) + \frac{1}{M} \eta_j(t) \\ & - \frac{\gamma(t)}{M} \nu_{jk} X_k(0) - \int_0^{\infty} dt' \frac{\gamma(t-t')}{M} \nu_{jk} \dot{X}_k(t'). \end{aligned} \quad (5)$$

The matrix C is the coupling matrix of the isolated chain

$$C_{jk} = \left(\omega_j^2 + \frac{f_{j+1} + f_j}{M} \right) \delta_{jk} - \frac{f_{j-1}}{M} \delta_{j-1,k} - \frac{f_j}{M} \delta_{j+1,k},$$

with f_0 and f_l set to zero. $\eta_j(t)$ and $\gamma(t)$ are the noise function and the damping function and are discussed below. The matrix $\nu_{jk} = \delta_{jk} (\delta_{j1} + \delta_{jl})$ connects the damping term to the first and the last oscillator of the chain.

a. The damping function The damping kernel has the form

$$\gamma(t-t') = \sum_{i=1}^N \frac{c_i^2}{m_i \omega_i^2} \cos(\omega_i(t-t')). \quad (6)$$

If we choose the coupling constants c_i according to the Drude-Ullersma-spectrum [8]

$$c_i = \sqrt{\frac{2\gamma m_i \omega_i^2 \Delta}{\pi} \frac{\Gamma^2}{\omega_i^2 + \Gamma^2}} \quad (7)$$

and perform the limit $N \rightarrow \infty$ and $\Delta \rightarrow 0$, we get the convenient result $\gamma(t) = \gamma \Gamma e^{-\Gamma|t|}$ with the Laplace transform $\hat{\gamma}(s) = \frac{\gamma \Gamma}{\Gamma + s}$.

b. The noise functions η_a and η_b act on the first, respectively on the last oscillator of the chain

$$\eta_j(t) := \eta_a(t) \delta_{j1} + \eta_b(t) \delta_{jl}. \quad (8)$$

The noise is determined by the initial conditions of the respective heat bath

$$\eta_\alpha(t) := \sum_{i=1}^N c_i \left[x_{\alpha i}(0) \cos(\omega_i t) + \frac{p_{\alpha i}(0)}{m_i \omega_i} \sin(\omega_i t) \right], \quad (9)$$

$\alpha = a, b$. In contrast to the damping, the noise functions depend on the temperature of the respective bath. The random character of the noise function comes from the unknown initial conditions of the bath degrees of freedom. As the initial conditions $x_i(0)$ and $p_i(0)$ have zero average, the average of $\eta_j(t)$ is also zero. Later we will need the symmetrical autocorrelation function of $\eta_\alpha(t)$, which is calculated using the initial conditions:

$$\begin{aligned} K_\alpha(t-t') &:= \frac{1}{2} (\langle \eta_\alpha(t) \eta_\alpha(t') \rangle + \langle \eta_\alpha(t') \eta_\alpha(t) \rangle) \\ &= \frac{1}{\pi} \int_0^{\infty} d\omega \gamma \hbar \omega \frac{\Gamma^2}{\Gamma^2 + \omega^2} \coth \left(\frac{\hbar \omega}{2k_B T_\alpha} \right) \cos(\omega(t-t')) \end{aligned} \quad (10)$$

There is no analytical expression for this integral. It is nonzero even for $T_\alpha = 0$, indicating that quantum fluctuation are never absent. In the classical limit $\coth \left(\frac{\hbar \omega}{2k_B T_\alpha} \right)$ reduces to $2k_B T_\alpha / (\hbar \omega)$, and in the Markovian limit $\Gamma \rightarrow \infty$, K_α in equation (10) becomes δ -like, which means white noise. A detailed discussion of quantum noise can be found e. g. in [12].

It is worth mentioning that the Heisenberg equations of motion for the operators are identical with the classical equations of motion. All quantum mechanical effects follow from the initial conditions of the chain and of the bath degrees of freedom in the noise function.

2. The solution of the Langevin equations

Thanks to the linearity of the problem the equations of motion (5) can be easily solved in Laplace space, where the convolution turns into a product and the differential equation becomes algebraic. By using the Laplace transform instead of the Fourier transform used in [9], we will be able to solve equation (5) for any t and not only for the stationary case. In Laplace space the equation reads

$$\begin{aligned} s^2 \hat{X}_j(t) - s X_j(0) - \frac{P_j(0)}{M} = & -C_{jk} \hat{X}_k + \frac{\hat{\eta}_j(s)}{M} \\ & - \nu_{jk} \frac{s \hat{\gamma}(s)}{M} \hat{X}_k(s). \end{aligned} \quad (11)$$

We perform a coordinate transformation to the eigenfunctions Y_i of the coupling matrix C , i. e. to the normal coordinates of the isolated chain, which are standing waves in the case of the ordered chain. The transformation matrix is denoted by G : $X_i = G_{ij}Y_j$, $(GCC^t)_{ij} = \Omega_i\delta_{ij}$. The equations of motion then read

$$\hat{B}_{ij}(s)\hat{Y}_j(s) = sY_i(0) + \frac{Q_i(0)}{M} + \frac{G_{1i}\hat{\eta}_a(s) + G_{li}\hat{\eta}_b(s)}{M}, \quad (12)$$

with the interaction matrix

$$\hat{B}_{ij}(s) := \left[(s^2 + \Omega_j^2)\delta_{ij} + \frac{s\hat{\gamma}(s)}{M} (G_{1i}G_{1j} + G_{li}G_{lj}) \right]. \quad (13)$$

Both damping and noise act on the normal coordinates

$$Y_j(t) = \sum_{k=1}^l \left[\dot{A}_{jk}(t)Y_k(0) + \frac{1}{M}A_{jk}(t)Q_k(0) \right] + \frac{1}{M} \int_0^t dt' [F_j^a(t-t')\eta_a(t') + F_j^b(t-t')\eta_b(t')], \quad (14)$$

with the response functions $F_j^a(t) = \sum_k A_{jk}(t)G_{1k}$ for the noise $\eta_a(t)$ and $F_j^b(t) = \sum_k A_{jk}(t)G_{lk}$ for $\eta_b(t)$. The equation for the momenta $Q_j(t) = M\dot{Y}_j(t)$ is obtained by differentiating. The response functions are sums of decaying exponential functions, e. g.

$$F_j^\alpha = \sum_k F_{j,k}^\alpha e^{\lambda_k t} + c.c. , \quad \text{Re}(\lambda_k) < 0 , \quad \alpha = a, b. \quad (15)$$

That means, any contribution from the initial conditions $Y(0)$ and $Q(0)$ vanishes with time. As mentioned above,

$$\begin{aligned} \frac{1}{2} \langle \{Y_i(t), Y_j(t)\} \rangle &= \sum_{k,n} \left[\dot{A}_{ik}(t)\dot{A}_{jn}(t) \langle Y_k(0)Y_n(0) \rangle + \frac{1}{M^2}A_{ik}(t)A_{jn}(t) \langle Q_k(0)Q_n(0) \rangle \right. \\ &\quad \left. + \frac{1}{M} \left(\dot{A}_{ik}(t)A_{jn}(t) + A_{ik}(t)\dot{A}_{jn}(t) \right) \frac{1}{2} \langle \{Y_n(0), Q_k(0)\} \rangle \right] \\ &\quad + \frac{1}{M^2} \int_0^t dt' \int_0^{t'} dt'' \left[F_i^a(t-t')F_j^a(t-t'')K_a(t'-t'') + F_i^b(t-t')F_j^b(t-t'')K_b(t'-t'') \right] \end{aligned} \quad (16)$$

The generalization to time-shifted correlations is straight forward.

In the integral there is a summation over the exponentials $\exp(\lambda_k(t-t'))$ and $\exp(\lambda_{k'}(t-t''))$ from (15) and the ω -integration in $K(t'-t'')$ (see (10)). The dou-

ble time integration over exponentials and cosines can be performed analytically. In the limit $t \rightarrow \infty$ it yields the result

$$\frac{\lambda_k\lambda_{k'} + \omega^2}{(\lambda_k^2 + \omega^2)(\lambda_{k'}^2 + \omega^2)} .$$

via G_{1i} and G_{li} , i. e. their deflections at the ends, where the chain is coupled to the baths.

We need the inverse of the interaction matrix $\hat{B}(s)$ for resolving (12) for $\hat{Y}_j(s)$. The entries of $\hat{B}(s)$ are rational functions of s . We extract the common divisor of all matrix entries and end up with a matrix containing only polynomial entries, which can be inverted using Cramer's rule. The entries of $\hat{A} = \hat{B}^{-1}$ are rational functions of s with a common denominator, where the poles lie in the left half of the complex plane. After performing a partial fraction expansion we transform back to time space. In the case of symmetric chains we will have a closer look at the inversion of the matrix $\hat{B}(s)$, in Appendix A.

Inverting equation (12) and transforming to time space thus yields

the averages $\langle \eta_a(t) \rangle$ and $\langle \eta_b(t) \rangle$ are zero, so $\langle Y_j(t) \rangle$ is zero, as well. Two-point-correlations of coordinates and momenta are the objects of interest.

3. The evaluation of time dependent correlations

With the response functions $A_{jk}(t)$ and $F_j^\alpha(t)$, and the symmetrical autocorrelation functions $K_\alpha(t-t')$ of the noise provided, one can evaluate any symmetrical correlation like $\frac{1}{2} \langle \{Y_i(t), Y_j(t)\} \rangle$ or $\frac{1}{2} \langle \{Y_i(t), Q_j(t)\} \rangle$. E. g.

Then the ω -integrations are evaluated for each pair of roots $(\lambda_k, \lambda_{k'})$ and summed up.

Beside calculating the roots λ_k and the coefficients for the response functions $F_{j,k}^\alpha$ (15), the evaluation of the ω -integrals is the main numerical work.

B. Symmetric disordered chains

In this section we consider a specialization of the system above, namely a disordered chain with left-right symmetry, which means that the Hamiltonian is invariant under the exchange $X_n \rightarrow X_{l+1-n}$. This implies $f_n = f_{l-n}$ and $\omega_n = \omega_{l+1-n}$. The normal coordinates of H_{ch} are either symmetric or antisymmetric with respect to commuting left and right. In particular the transformation matrix G and the noise response functions obey the following relations

$$\begin{aligned} Y_i \text{ even} &\Rightarrow G_{1i} = G_{li} \Rightarrow F_i^a(t) = F_i^b(t) \\ Y_j \text{ odd} &\Rightarrow G_{1j} = -G_{lj} \Rightarrow F_j^a(t) = -F_j^b(t). \end{aligned} \quad (17)$$

Even modes thus respond to the effective noise $\eta_e = \eta_a + \eta_b$ and odd ones to $\eta_o = \eta_a - \eta_b$. The nondiagonal terms in $\hat{B}(s)$ are proportional to $(G_{1i}G_{1j} + G_{li}G_{lj})$ and vanish, if the corresponding modes have different symmetry. This implies that the interaction matrix $\hat{B}_{ij}(s)$ in (12) and its inverse A are block matrices which do not mix even and odd modes. Therefore the matrix inversion can be solved for each symmetry family separately with separate sets of roots.

For convenient notation we define the symmetry function $p(j)$ and the symmetry family $\sigma(j)$

$$p(j) := \begin{cases} e & \text{for } Y_j \text{ even} \\ o & \text{for } Y_j \text{ odd} \end{cases} \quad (18)$$

$$\sigma(j) := \{i \mid p(i) = p(j)\}. \quad (19)$$

With $\hat{F}_j^a(s) := \hat{F}_j^a(s)$ one can express equation (14) in the following compact form

$$\begin{aligned} Y_j(t) = & \sum_{k \in \sigma(j)} \left[\dot{A}_{jk}(t) Y_k(0) + \frac{1}{M} A_{jk}(t) Q_k(0) \right] \\ & + \frac{1}{M} \int_0^t dt' F_j(t-t') \eta_{p(j)}(t'). \end{aligned} \quad (20)$$

The noise response functions read

$$F_j(t) = \sum_{i \in \sigma(j)} F_{ji} e^{\lambda_i t}. \quad (21)$$

Only exponentials with λ_i from the same symmetry as Y_j occur.

C. Ordered Chains

A further specialization of the disordered chain is to set all couplings f_n equal to a constant f and all ω_n to

ω_0 . In this case the normal coordinates of the isolated chain are simply standing waves with anti-nodes at the ends.

III. RESULTS

In this chapter we present and discuss some numerical results obtained with the techniques presented in the previous chapter. We set the mass M , the Planck constant \hbar and the Boltzmann constant k_B to one and fix the cutoff $\Gamma = 10$. Unless specified otherwise we choose a chain with length $l = 20$. In section III A the couplings f_i are set to one and in section III B disorder in the f_i is introduced.

The onsite frequencies ω_i are kept as simple as possible. They cannot be set to zero because the translation of the center-of-mass must be suppressed. We set all ω_i to one, that means, our chain is fixed on a substrate and cannot move macroscopically. Another possibility, often employed in the literature [4, 13, 14], is to fix only the first and the last oscillator with an onsite potential, corresponding to a free wire spanned between the heat baths. At some points we will refer to this model as well.

Except for section III D, we will focus on the correlations within the coordinates and momenta of the chain in the stationary regime, i. e. the initial conditions of the chain are irrelevant.

A. Ordered Chains

In contrast to chapter II, where we started with the general disordered case and specialized the system till the ordered chain, we will begin with the simplest case, the ordered chain, here.

1. Energy distribution in the normal coordinates

As the calculation of the variances is performed in normal coordinates, we inspect the energy distribution in normal coordinates first. The energy in the normal coordinates of the unperturbed chain reads $E_i = \frac{1}{2} M \Omega_i \langle Y_i^2 \rangle + \frac{1}{2M} \langle Q_i^2 \rangle$. As the coupling to the heat baths is rather strong, we take the coupling energy into account by determining effective frequencies. Therefore we perform a second calculation with both bath temperatures set to zero, i. e. the entire system will be in the ground state. We then identify the groundstate energy with the zero point energy of an oscillator with the effective frequency $\tilde{\Omega}_i$. Furthermore we assume that the virial theorem is approximately valid, although the normal coordinates of the unperturbed chain are coupled among each other by the interaction with the baths. Therefore one can calculate an effective frequencies $\tilde{\Omega}_i$ using only

the kinetic energies $\langle Q_i^2 \rangle / (2M)$

$$(E_0)_i \approx 2(E_0^{\text{kin}})_i = \frac{\langle Q_i^2 \rangle_0}{M} = \frac{1}{2} \hbar \tilde{\Omega}_i$$

Then we use the effective frequencies $\tilde{\Omega}_i$ to calculate the occupation numbers from the kinetic energies at finite temperatures:

$$n_i = \frac{\langle Q_i^2 \rangle_0 / M}{\hbar \tilde{\Omega}_i} - \frac{1}{2}$$

The low frequency modes with large amplitudes at the ends of the chain are affected the most by the coupling to the baths.

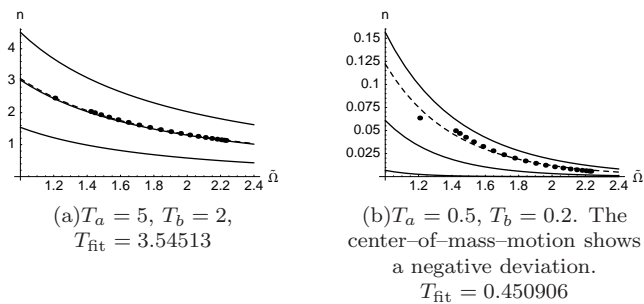


FIG. 1: Occupation numbers of the normal modes calculated from the kinetic energies. Parameters: $f = 1$, $\gamma = 2$

In Fig. 1 these occupation numbers are plotted. Although there is a temperature difference and a heat flux between left and right (see Sec. III A 3), the occupation numbers essentially agree with the Bose-Einstein distributions $\left[\exp\left(\frac{\hbar \tilde{\Omega}}{k_B T_{\text{fit}}}\right) - 1 \right]^{-1}$ in both cases. In the high temperature case (a), T_{fit} agrees with the average temperature $(T_a + T_b)/2$. In the low temperature case (b), the temperature T_{fit} is closer to the higher bath temperature, giving a hint to the fact that the heat conductivity increases with temperature (III A 3). There are some deviations from the Bose-Einstein distribution resulting from the approximations made in the calculation of the frequencies. In the limit of weak coupling they vanish.

Different definitions of effective frequencies are possible. For example one could use the potential energies instead of the kinetic energies and would obtain different results. The reason for this is that the normal coordinates of the unperturbed system are coupled via the heat baths. We are not dealing with independent oscillators in the ground state, which is reconfirmed by the fact that we find $\langle Y_i^2 \rangle_0 \langle Q_i^2 \rangle_0 > \left(\frac{\hbar}{2}\right)^2$.

2. Temperature profiles

We transform the correlations of the normal coordinates back to real space and calculate the energy per

site, splitting each spring energy to the neighboring sites

$$E_n = \frac{\langle P_n^2 \rangle}{2M} + \frac{1}{2} (M\omega_n^2 + f_{n-1} + f_n) \langle X_n^2 \rangle - f_{n-1} \langle X_n X_{n-1} \rangle - f_n \langle X_n X_{n+1} \rangle. \quad (22)$$

Numerical results are shown in Fig. 2. The energies of the first and the last oscillator are close to the thermal energies of the respective heat bath, and like in the classical investigations (e. g. [4]), the temperature gradient vanishes inside the chain. With different coupling parameters f and γ one can change the behavior only very close to the boundaries. In the low temperature case the energies per site are dominated by the zero-point energies. The energies of the boundary oscillators are elevated because their effective frequencies are increased by the coupling to the heat baths.

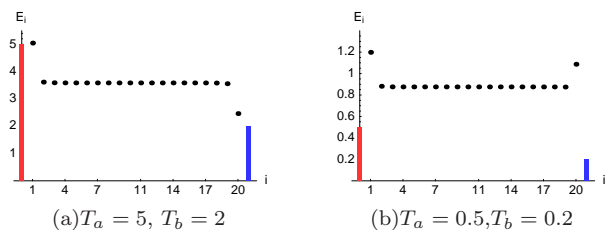


FIG. 2: Energy per site (dots). The bars represent the thermal energies of the respective heat baths. Parameters: $f = 1$, $\gamma = 2$

We want to eliminate the zero-point energies and construct a temperature for each lattice site. Like in the previous section we determine effective frequencies with a ground state calculation, using $E_0 = \hbar \tilde{\omega} / 2$. Then we assign a temperature T_R using $E = \frac{1}{2} \hbar \tilde{\omega} \coth\left(\frac{\hbar \tilde{\omega}}{2k_B T_R}\right)$.

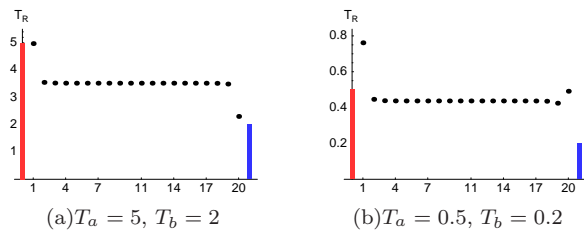


FIG. 3: The temperatures T_R reconstructed from the energies per site and the zero-point energies per site. The bars represent the temperatures of the respective heat baths. Parameters: $f = 1$, $\gamma = 2$

In Fig. 3 the reconstructed temperature is shown. In the high temperature case (a) the result looks rather the same as in Fig. 2, because the zero-point energies are not very relevant at high temperatures. In the low temperature case (b) however, the zero-point energies have been compensated and one can see a temperature profile which lies between the two bath temperatures, except for the boundary oscillators. Again the temperature gradient is

only an exponentially small boundary effect. Note that the interior temperature is again closer to the temperature of the warm heat bath, indicating a higher thermal conductivity at high temperatures.

3. The heat flux

We set up an equation of energy continuity

$$\frac{d}{dt}E_n = J_{n-1,n} - J_{n,n+1} \quad (23)$$

by differentiating (22). In the stationary case we find for the energy fluxes from site n to $n+1$

$$J_{n,n+1}^\infty = \frac{f_n}{M} \langle X_n P_{n+1} \rangle. \quad (24)$$

This result agrees with the classical formula ‘power = force \times velocity’ using ‘force = $f_n(X_{n+1} - X_n)$ ’ and $\langle X_n P_n \rangle \propto \frac{d}{dt} \langle X_n^2 \rangle = 0$.

Due to energy conservation $J_{n,n+1}^\infty$ must be independent of n , therefore we write $J := J_{n,n+1}^\infty$. The heat flux J is one scalar quantity and therefore easier to analyze than the temperature gradient.

a. Heat flux as a function of the coupling constants We calculate the heat flux for different coupling constants f and γ and plot the heat flux over the f - γ -plane, see Fig. 4. In general the heat flux grows with f and γ , but

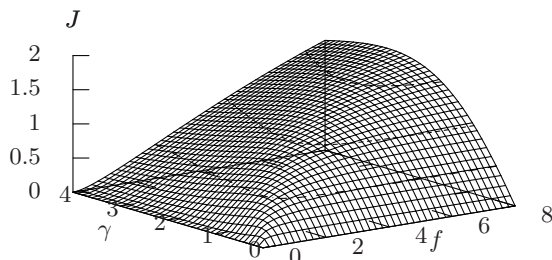


FIG. 4: The heat flux J as a function of the coupling to the heat baths γ and the coupling within the chain f . $T_a = 5$, $T_b = 2$

f and γ must be tuned to each other. If f is between two and three times as big as γ , the heat flux is particularly high.

b. Heat flux and chain length In the case of normal heat conduction the heat flux is expected to decrease reciprocal with the chain length at fixed temperature difference $T_a - T_b$. In agreement with the vanishing temperature gradient inside the chain (Sec. III A 2), we find that the heat flux does not decrease with the chain length for $l \gtrsim 5$, Fig. 5. The total heat conductivity rather than the specific conductivity is a constant in the ordered harmonic chain.

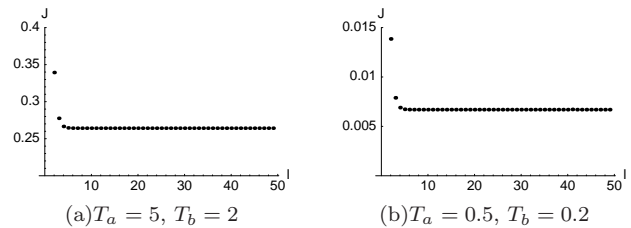


FIG. 5: The heat flux as a function of the chain length l . Parameters: $\gamma = 2$, $f = 1$

c. Thermal conductivity as a function of temperature We are especially interested in the low temperature regime. Therefore we vary the mean temperature with a fixed relative temperature difference $\epsilon = (T_a - T_b)/(T_a + T_b)$ and calculate the conductivity $G_{\text{th}} := J/(T_a - T_b)$ for each temperature.

Results are shown in Fig. 6. In the high temperature regime the conductivity is a constant like in the classical case. In the low temperature regime it breaks down and behaves similarly to the Bose-Einstein occupation numbers of the lowest normal frequencies (gray line). In this case the degrees of freedom of the chain are simply frozen out.

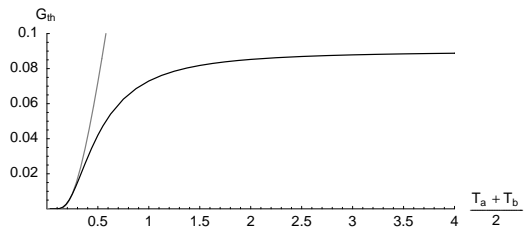


FIG. 6: Black: The thermal conductivity as a function of temperature. Gray: $c [\exp(\hbar\omega_0/k_B T) - 1]^{-1}$. Parameters: $\epsilon = 0.01$, $f = 1$, $\gamma = 2$

This behavior is typical for optical phonons. In our model the low normal frequencies start with the value ω_0 , that means all normal modes are frozen if $k_B T \lesssim \hbar\omega_0$. If we set ω_0 to zero in the inner chain, the normal frequencies start at zero and we find the temperature dependence of acoustic phonons $G_{\text{th}} \propto T^3$, which was also found in [14].

B. Disordered Chains

It is well known from classical works that disorder can lead to a finite temperature gradient inside the chain, e. g. [2, 4]. Temperature profile, heat flux etc. are calculated for many realizations of disorder and averaged over. In the following $\langle \cdot \rangle$ denotes the ensemble average. There are different possibilities to bring disorder into play:

- A common choice in the literature is to choose

the masses of the oscillators randomly. This corresponds to isotopical disorder in nature.

- Random frequencies of the onsite potentials ω_i
- Random coupling constants f_i between the oscillators of the chain.

To simplify matters we confine ourselves to disorder in the couplings f_i in this article. The f_i are chosen from a Gaussian distribution with mean \bar{f} and width σ_f , and a cutoff that guarantees that the f_i are always positive. In the following we use the notation $f = \bar{f} \pm \sigma_f$.

As indicated in II B, the symmetry of the chain is relevant. Therefore we always compare the results of the symmetrical and the unsymmetrical disordered chain in this subsection.

1. Normal modes in disordered chains

The disorder changes the normal modes from standing waves to localized states. As we are considering disorder in the couplings f_i , the high frequency modes are affected the most by disorder. We calculate the localization length ξ in units of the lattice constant as the inverse of the participation number p :

$$\xi_i := p_i^{-1} := \left[\sum_{j=1}^l Y_{ij}^4 \right]^{-1} \quad (25)$$

The center-of-mass mode, which is extended over the whole chain yields $\xi = l$, a fully localized mode yields $\xi = 1$. Results for an unsymmetrical disordered chain are shown in Fig. 7. The center-of-mass mode has $\xi = l$, all the other modes have smaller localization lengths, which decrease with frequency.

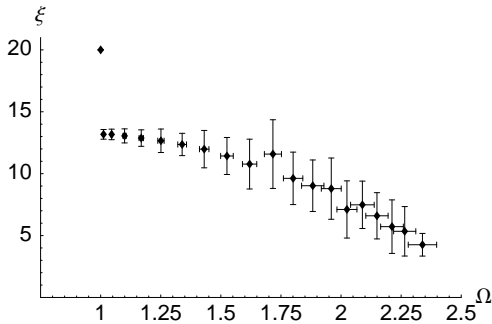
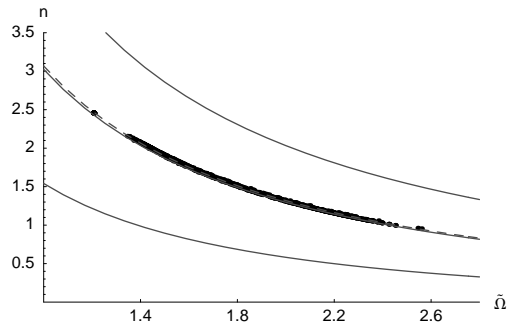


FIG. 7: The localization length ξ in dependence of normal frequencies Ω for an unsymmetrical chain with $f_i = 1 \pm 0.2$ averaged over 50 realizations, the error bars show the standard deviation.

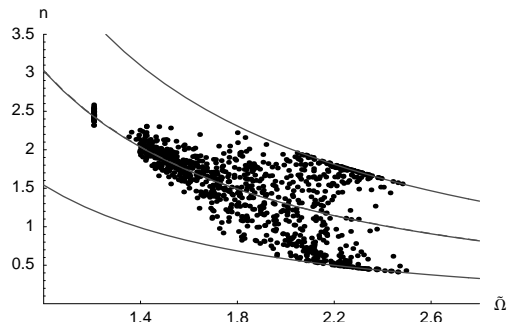
In the symmetric chain the normal modes are constrained to be symmetric or antisymmetric, and are therefore less localized.

2. Occupation numbers

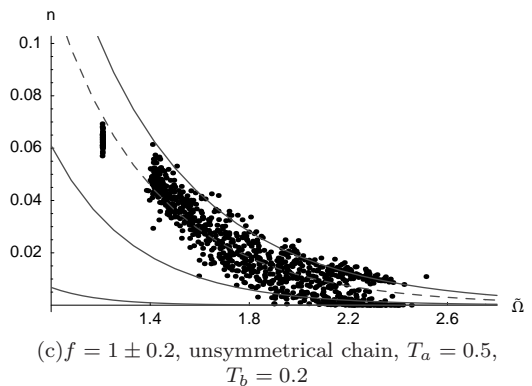
In Fig. 8 the occupation numbers of disordered chains are shown. In the symmetrical chain the frequencies are smeared by disorder, compared to the ordered case in Fig. 1 (a). At the same time the occupation numbers still agree with the Bose-Einstein distribution at the mean temperature.



(a) $f = 1 \pm 0.2$, symmetrical chain, $T_a = 5$, $T_b = 2$



(b) $f = 1 \pm 0.2$, unsymmetrical chain, $T_a = 5$, $T_b = 2$



(c) $f = 1 \pm 0.2$, unsymmetrical chain, $T_a = 0.5$, $T_b = 0.2$

FIG. 8: Occupation numbers from 50 realizations of disorder. The lines show Bose-Einstein distributions corresponding to the mean temperature $(T_a + T_b)/2$, to the bath temperatures T_a and T_b and to the average temperature of the normal modes (dashed). Parameters: $\omega_0 = 1$, $\gamma = 2$, $T_a = 5$, $T_b = 2$

In the unsymmetrical case, Fig. 8 (b), this changes: The distribution broadens and the points lie between the Bose-Einstein distributions corresponding to T_a and T_b .

It is striking that the points belonging to the high frequency modes tend to lie close to either bath temperature. This is due to the fact that the strongly localized high-frequency modes are not restricted to be symmetric or antisymmetric any more. Therefore they are coupled much more strongly to the bath they lie closer to.

3. Temperature profile and heat flux

Again we transform to real space and calculate the energy distribution. There are great differences between the single realizations of disorder, so one has to average over many realizations in order to obtain comparable results, see Fig. 9. On average the temperature gradient is enhanced in the disordered chain. In the unsymmetrical case the distribution is much wider and the average temperature gradient is steeper. The low tempera-

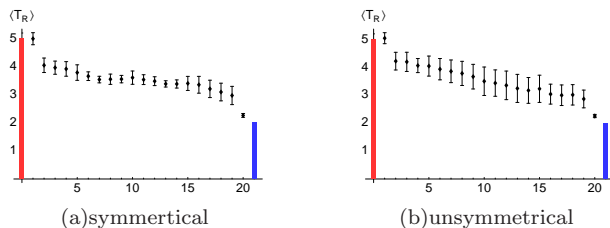


FIG. 9: Temperature profile averaged over 50 realizations. The error bars show the standard deviation of the temperature at each lattice site. Parameters: $f = 1 \pm 0.2$, $l = 20$, $\omega_0 = 1$, $\gamma = 2$, $T_a = 5$, $T_b = 2$

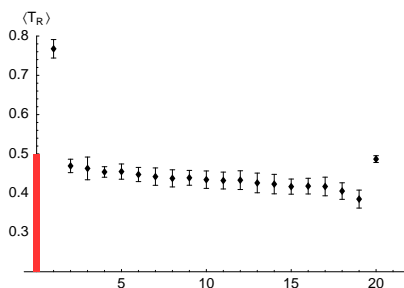


FIG. 10: Temperature profile in the unsymmetrical case averaged over 50 realizations. In the symmetrical case the temperature gradient is about half as steep. Parameters: $f = 1 \pm 0.2$, $l = 20$, $\omega_0 = 1$, $\gamma = 2$, $T_a = 0.5$, $T_b = 0.2$

ture disordered case, Fig. 10 (a) is similar to the ordered case. The difference between the temperature profile in the symmetrical and in the unsymmetrical case is still visible, but very small (b).

The heat flux is reduced in the disordered case, compare Fig. 11 and Fig. 5 (a). The main difference compared to the ordered case (see Fig. 5) is, that the heat flux is not independent of the chain length for $l \gtrsim 5$ any

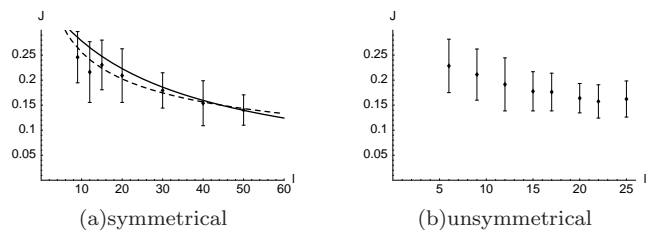


FIG. 11: Mean heat current as a function of the chain length l . The errorbars show the width of the current distribution. Each point represents between 28 and 100 realizations of disorder. In (a) two fits are plotted, see text. Parameters: $\omega_0 = 1$, $\gamma = 2$, $T_a = 5$, $T_b = 2$, $f = 1 \pm 0.2$

more. In the symmetrical case it was possible to calculate the correlations for a chain length up to $l = 50$ in a reasonable time. In Fig. 11 there are two fits plotted. The solid line shows the function $0.37/(1 + 0.033l)$, which corresponds to normal heat conduction, i. e. a heat resistance proportional to the chain length plus a contact resistance. The dashed line shows the function $0.7/(1 + 0.55\sqrt{l})$, which corresponds to the classical result of a heat resistance proportional to the root of the chain length plus a contact resistance, as it was found in [2] for a different disordered model. Due to the wide distribution of the heat currents and the finite lengths of the considered chains, we cannot definitely decide which fit describes the asymptotic behavior better.

C. Entanglement

Beside the zero point energies and the Bose–Einstein statistics of the occupation numbers, entanglement is another relevant quantum mechanical feature that can be observed in our model.

We use the logarithmic negativity, which is a measure for the entanglement between two parts of a system, that can be calculated from the correlations between the coordinates and momenta of the system.

We set up the covariance matrix containing all the correlations between coordinates and momenta in real space. Then the system is divided into two parts \mathcal{A} and \mathcal{B} and the covariance matrix is partially transposed with respect to \mathcal{B} . The logarithmic negativity is then given by

$$N = - \sum_j \log_2(\min(1, |\gamma_j|)) , \quad (26)$$

where the γ_j are the symplectic eigenvalues of the partially transposed covariance matrix, see [15, 16]. We use the notation N_k for the logarithmic negativity of the subsystems $\mathcal{A} = \{X_1, \dots, X_k\}$ and $\mathcal{B} = \{X_{k+1}, \dots, X_l\}$. Other divisions, e. g. taking every second oscillator or performing the division in normal mode space, are also possible, but their physical meaning is not obvious.

1. Entanglement in dependence of the couplings f and γ

We start with the ordered case. Fig. 12 shows the entanglement for different divisions of a chain of length 20 as a function of the coupling within the chain f . With $f = 0$ the oscillators are not coupled at all and there is no entanglement. Increasing f favors entanglement. For each N_k there is a threshold coupling where entanglement starts. In N_1 and N_{l-1} one of the subsystems is a single oscillator at the end of the chain coupled directly to a bath. In this case we observe a lower logarithmic negativity and a higher threshold coupling for the onset of entanglement. All the other N_k with $1 < k < l - 1$ behave very similarly.

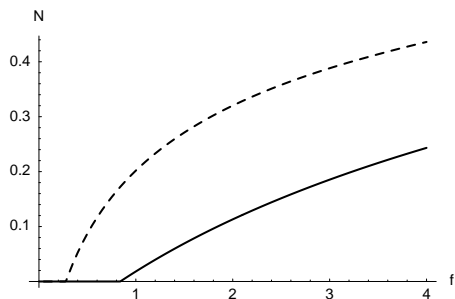


FIG. 12: Stationary logarithmic negativity as a function of the coupling f inside the ordered chain. Solid line: N_1 , dashed line: N_5 . Parameters: $l = 20$, $\gamma = 2$.

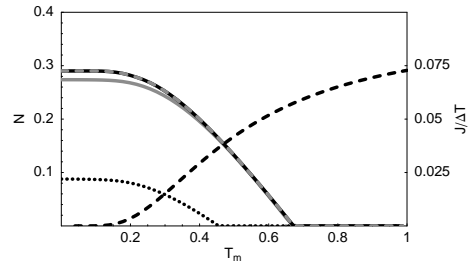
2. Entanglement as a function of temperature

We expect the logarithmic negativity to decrease and finally vanish with increasing temperature. Additionally to the ordered case we want to investigate the entanglement in the unsymmetrical disordered case. Therefore we vary the mean temperature $T_m = (T_a + T_b)/2$ for each realization of disorder. Another quantity marking the transition from the quantum mechanical regime is the heat conductivity (see Sec. III A 3) which will be observed simultaneously.

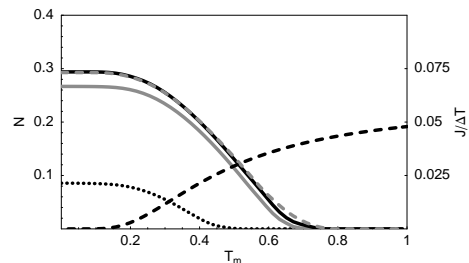
T_a and T_b are chosen as $(1 \pm \epsilon)T_m$ with $\epsilon = 0.1$. The further parameters are chosen

$$l = 20 \quad \Gamma = 10 \quad \gamma = 2 \quad \bar{f} = 1 \quad \sigma_f = 0.2 \quad \omega_0 = 1. \quad (27)$$

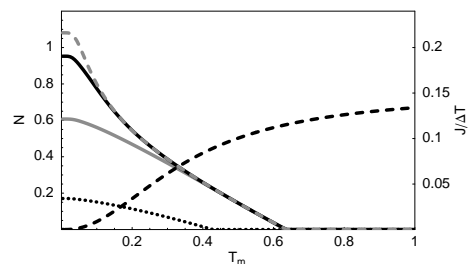
In Fig. 13 (a) the conductivity and entanglements for different divisions of the chain are plotted for an ordered chain. The entanglements with one subsystem consisting of a single oscillator N_1 and N_{19} have lower values than the others, as observed already in the previous section. All N_k are initially constant and start decreasing at $T_m \approx 0.2$. N_1 and N_{19} reach zero at $T_m \approx 0.45$, the others follow at $T_m \approx 0.67$. In the same temperature range the heat conductivity rises.



(a) Ordered Chain, $\epsilon = 0.1$



(b) Unsymmetrical disordered chain, $f = 1 \pm 0.2$, averaged over 20 realizations, $\epsilon = 0.1$



(c) Ordered Chain, no onsite potential within the chain, $\epsilon = 0.01$

FIG. 13: The heat conductivity $J/\Delta T$ (dashed line) and some entanglements and as a function of temperature. Dotted line: N_1 ; gray line: N_2 ; solid line: N_5 ; gray dashed line: N_{10} . Parameters from (27)

In the disordered case (Fig. 13 (b)) there are only minor changes to the entanglement in each realization of disorder. The sharp transition to zero is washed out by the average. As seen before the heat conductivity $J/\Delta T$ is lower in the disordered case, but it shows essentially the same temperature dependence.

The plateau we observe at low temperatures result from the frequencies of the normal modes starting from ω_0 . In the case of a chain with onsite potentials only at the ends of the chain, Fig. 13 (c), the logarithmic negativity reaches higher values at low temperatures, but their decrease starts already at lower temperatures.

D. Time evolution

Finally we shortly want to study some time dependencies of the system. For simplicity we inspect a short ordered chain, consisting of only four oscillators. We evaluate the time dependent correlations (like equation (16)) and study e. g. the diagonal momentum correlations, which are proportional to the kinetic energy, see Fig. 14. Under some oscillations each lattice site gains

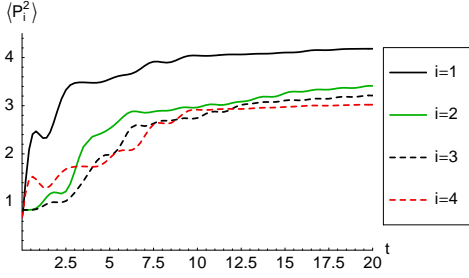


FIG. 14: The time evolution of the diagonal momentum correlations. Parameters: $f = 1$, $\gamma = 0.5$, $T_a = 5$, $T_b = 2$

energy until it reaches the value corresponding to the stationary temperature profile.

Furthermore we generalize equation (16) for correlations of two coordinates or momenta at different times. In Fig. 15 results are shown for the time shifted autocorrelation functions of the momenta of the normal coordinates in the stationary limit. Each correlation performs damped oscillations with its slightly detuned frequency. Each normal coordinate loses energy by damping which is replaced by incoherent noise. The stronger the influence of damping and noise to a normal coordinate, the faster it loses memory of its history and the autocorrelation function decays. Normal modes with large amplitudes at the ends of the chain experience the strongest damping.

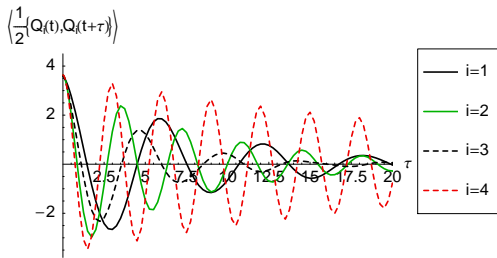


FIG. 15: The time shifted diagonal momentum correlations in normal coordinates in the limit $t \rightarrow \infty$. Parameters like in Fig. 14

IV. SUMMARY AND CONCLUSIONS

We have treated disordered harmonic chains with the Quantum Langevin formalism in the strong coupling regime. The strong coupling to the heat baths led to a renormalization of the normal frequencies. In ordered chains the occupation numbers calculated with these frequencies approximately follow the Bose–Einstein statistics, even in the strong–coupling non–equilibrium regime. The heat flux follows from non–diagonal correlations between coordinates and momenta.

Symmetric disorder does not change the occupation numbers qualitatively, because the normal coordinates are constrained to have the same amplitude at both ends of the chain.

With breaking the left–right symmetry this changes. The localization of most of the modes enhances the effect of strongly asymmetric coupling to the heat baths.

In the low temperature regime the energy distribution in the chain is dominated by zero–point energies that have to be taken into account for constructing the local temperature T_R . In the limit of ordered chains we have recovered the length–independent heat flux known from classical models. In disordered chains the heat flux decreases with the length, but the asymptotic behavior could not be identified due to numerical restrictions.

Characteristic quantum mechanical features are the freezing of the heat conductivity, that behaves typical for optical phonons in our model. In the same temperature range where the heat conductivity freezes, entanglement appears.

Appendix A: THE NOISE RESPONSE FUNCTIONS IN THE SYMMETRICAL CASE

We want to calculate only the noise response functions and therefore omit the initial conditions in (12). We use the symmetry relations (17) and get

$$(s^2 + \Omega_i^2) \hat{Y}_i(s) + \sum_{j \in \sigma(i)} 2G_{1i} G_{1j} \frac{s \hat{\gamma}(s)}{M} \hat{Y}_j(s) = \frac{G_{1i}}{M} \hat{\eta}_{p(i)}(s) \quad (\text{A1})$$

Dividing this equation by G_{1i} and subtracting the same equation with $i = n$ yields

$$\frac{(s^2 + \Omega_n^2) \hat{Y}_n(s)}{G_{1n}} = \frac{(s^2 + \Omega_i^2) \hat{Y}_i(s)}{G_{1i}}.$$

Using this equation for eliminating all \hat{Y}_j with $j \neq i$ from (A1) yields

$$\hat{Y}_i(s) = \frac{1}{M} \hat{F}_i(s) \hat{\eta}_{p(i)}(s), \quad (\text{A2})$$

with

$$\hat{F}_i(s) = \frac{G_{1i}}{(s^2 + \Omega_i^2)} \left[1 + \sum_{j \in \sigma(i)} \frac{2G_{1j}^2}{(s^2 + \Omega_j^2)} \frac{s \hat{\gamma}(s)}{M} \right]^{-1}.$$

Extracting the common denominator $\hat{D}_{p(i)}(s)$ yields the rather simple form

$$\hat{F}_i(s) = \frac{(s + \Gamma)G_{1i} \prod_{\substack{j \in \sigma(i) \\ j \neq i}} (s^2 + \Omega_j^2)}{\hat{D}_{p(i)}(s)}. \quad (\text{A3})$$

The numerator contains any $(s^2 + \Omega_j^2)$ from the same symmetry, except for the term with its own frequency. It is proportional to the amplitude of the mode at the end of the chain G_{1i} .

1. The roots of the denominator

The denominator of all response functions with the same symmetry reads

$$\begin{aligned} \hat{D}_{p(i)}(s) &= (s + \Gamma) \prod_{j \in \sigma(i)} (s^2 + \Omega_j^2) \\ &+ 2s \frac{\gamma \Gamma}{M} \sum_{j \in \sigma(i)} G_{1j}^2 \prod_{k \neq j} (s^2 + \Omega_k^2). \end{aligned} \quad (\text{A4})$$

In the following we will prove that the real parts of the roots of $\hat{D}_{p(i)}(s)$ are negative. As $s = \pm i\Omega_j$ and $s = 0$ are no roots, we can search for the roots of $\hat{D}_{p(i)}(s) / \left[\prod_{j \in \sigma(i)} (s^2 + \Omega_j^2) \Gamma s \right]$, which implies

$$\hat{u}(s) := \frac{1}{\Gamma} + \frac{2\gamma}{M} \sum_{k \in \sigma(i)} \frac{G_{1k}^2}{(s^2 + \Omega_k^2)} = -\frac{1}{s} \quad (\text{A5})$$

Without loss of generality we assume that $\text{Re}(s) > 0$. Now we assume $\text{Im}(s) > 0$, which implies $\arg(s) = \arg(-1/s) \in (0, \pi/2)$. On the other hand we find $\arg(s^2 + \Omega_j^2) \in (0, \pi) \Rightarrow \arg(1/(s^2 + \Omega_j^2)) \in (-\pi, 0) \Rightarrow \arg(\hat{u}(s)) \in (-\pi, 0)$. Therefore (A5) cannot be fulfilled and the assumption $\text{Im}(s) > 0$ is disproven.

-
- [1] E. Fermi, J. Pasta, and S. Ulam, Los Alamos Report **LA-1940** (1955).
- [2] A. Dhar, Phys. Rev. Lett. **86**, 5882 (2001), cond-mat/0105085.
- [3] F. Bonetto, J. L. Lebowitz, and L. Rey-Bellet, Fourier law: A challenge to theorists, math-ph/0002052, 2000.
- [4] S. Lepri, R. Livi, and A. Politi, Phys. Rep. **377**, 1 (2003), cond-mat/0112193.
- [5] A. V. Savin and O. V. Gendelman, Heat conduction in 1d lattices with on-site potential, cond-mat/0204631, 2002.
- [6] F. Bonetto, J. L. Lebowitz, and J. Lukkarinen, J. Stat. Phys. **116**, 783 (2004), math-ph/0307035.
- [7] P. Ullersma, Physica **32**, 27 (1966).
- [8] T. M. Nieuwenhuizen and A. E. Allahverdyan, Phys. Rev. E **66**, 36102 (2002).
- [9] A. Dhar and D. Roy, J. Stat. Phys. **125**, 801 (2006), cond-mat/0606465.
- [10] M. Michel, J. Gemmer, and G. Mahler, Physica E **29**, 129 (2005), cond-mat/0507642.
- [11] K. Saito, Europhys. Lett. **61**, 34 (2003).
- [12] C. W. Gardiner, *Quantum noise* (Springer, Berlin, 1991).
- [13] U. Zürcher and P. Talkner, Phys. Rev. A **42**, 3267 (1990).
- [14] U. Zürcher and P. Talkner, Phys. Rev. A **42**, 3278 (1990).
- [15] M. B. Plenio, J. Hartley, and J. Eisert, New J. Phys. **6**, 36 (2004), quant-ph/0402004.
- [16] G. Vidal and R. F. Werner, Phys. Rev. A **65**, 32314 (2002), quant-ph/0102117.
- [17] We use the Einstein notation, i. e. indices appearing twice are implicitly summed over.